Available online at www.sciencedirect.com
ScienceDirect
Journal of Molecular Catalysis A: Chemical 281 (2008) 119–125
JOURNAL OF MOLECULAR CATALYSIS A: CHEMICAL
www.elsevier.com/locate/molcata

Photodegradation of the herbicide 2,4-dichlorophenoxyacetic acid on nanocrystalline TiO_2–CeO_2 sol–gel catalysts

Félix Galindo [a], Ricardo Gómez [a,*], Manuel Aguilar [b]

[a] *Department of Chemistry, Universidad Autónoma Metropolitana-Iztapalapa, San Rafael Atlixco 186, A.P. 55-534, México City, D.F. 09340, Mexico*
[b] *Institute of Physics, Universidad Nacional Autónoma de México (UNAM), A.P. 20-364, 01000 México City, Mexico*

Available online 12 October 2007

Abstract

Nanocrystalline TiO_2–CeO_2 mixed oxides with different CeO_2 contents have been prepared by the sol–gel method. On the samples calcined at 673 K the specific surface areas, crystalline structures, optical absorption spectra and photocatalytic activity for the 2-dichlorophenoxyacetic acid degradation were determined. An important effect on the specific surface area as a function of the cerium oxide content was found; the BET areas increased from 73 m^2/g, for the bare TiO_2 catalyst, to 174 m^2/g on the catalysts containing 10 wt.% CeO_2. A continuous diminution in the energy of the E_g band gap, which varied from 3.14 eV, for TiO_2, to 2.47 eV for the catalysts with the highest cerium oxide content, was observed. The XRD Rietveld refinement showed that the number of the calculated $[V^{+}_{Ti^{4+}}]$ deficiencies diminished as the cerium oxide content increased. A strong dependence on the nanostructured crystallite size (8.4–33 nm) and the capacity for the herbicide photocatalytic degradation was observed. The highest activity corresponded to that of the catalysts with the smallest crystallite size.

Keywords: Titania–ceria mixed oxides; Titania–ceria sol–gel catalysts; 2,4-Dichlorophenoxyacetic acid photodegradation; Titania–ceria photocatalysts

1. Introduction

Titanium dioxide is currently considered as the most promising photocatalyst with successful results in the degradation of a large number of organic pollutants [1–5]. Additionally, an improved titania photo-efficiency when TiO_2 is combined with other oxides such as SnO_2 [6,7], ZrO_2 [8,9], Fe_2O_3 [10–12], Al_2O_3 [13], In_2O_3 [14,15], SiO_2 [16–18] or CeO_2 [19] has been reported. It has been found that the synthesis method employed for the formation of the mixed oxide exerts a strong influence on the photophysical and hence, on the photocatalytic properties showed by these materials. Therefore, a variety of methods have been developed for the synthesis of semiconductor mixed oxides. Among them, the hydrothermal, coprecipitation, impregnation, chemical vapor deposition and sol–gel methods have been mentioned frequently. The enhancement of the TiO_2 photoactivity by the second oxide has been attributed to the enlargement of the TiO_2 specific surface area, modifications in the titania crystallite size, the predominant crystalline phase, the modification in the band gap energy and the magnification of the TiO_2 crystalline defects.

In the present work, the preparation by the sol–gel method of the TiO_2–CeO_2 mixed oxides is reported. This technique was used since in previous works we reported a substantial modification of the photocatalytic activity of TiO_2 [20] by doping it with alkaline metals [21], iron oxides [22], sulfates [23] or indium oxides [24]. The selection of the cerium oxide and titania was done because of the important role of the Ce^{4+}/Ce^{3+} redox pair in heterogeneous oxidation catalytic reactions [25]. The work was aimed to study the effect of CeO_2 on the photophysical properties of TiO_2. The characterization of the TiO_2–CeO_2 mixed oxides was performed in order to determine the main variables that control the photocatalytic process. The specific surface area, titania crystallite size, crystalline phase composition and band gap energy were evaluated. The correlation among these textural, structural and photophysical properties with the photocatalytic

* Corresponding author. Tel.: +52 55 58044668; fax: +52 55 58044666.
E-mail address: gomr@xanum.uam.mx (R. Gómez).

1381-1169/$ – see front matter © 2007 Elsevier B.V. All rights reserved.
doi:10.1016/j.molcata.2007.10.008

decomposition of the herbicide 2,4-dichlorophenoxyacetic acid (2,4 D acid) was reported.

2. Experimental

2.1. Catalyst preparations

The TiO_2 and TiO_2–CeO_2 sol–gel catalysts were synthesized as follows: in a three neck flask containing an ethanol/water solution with a molar ratio of 16:8, the appropriate amount of cerium nitrate (Aldrich 99.9%) to obtain 2.5, 5.0, 7.5 and 10 wt.% CeO_2 in the final catalysts, was added. Afterwards, 1 mol of titanium *n*-butoxide (Aldrich 97%) was added dropwise during 1 h. Then, the solution was maintained in reflux until the gel was formed. After gelling, the samples were dried in air at 373 K; then, by increasing the temperature with a rate program of 2 K, the calcination temperature (673 K) was reached; temperature at which the samples were maintained for 4 h.

2.2. Characterization

2.2.1. Adsorption measurements

The nitrogen adsorption isotherms at 77 K were determined with an automatic Quantachrome Autosorb 3B instrument. Prior to the adsorption run, all the samples were outgassed overnight at 573 K. The N_2 and He gases required for the operation were UHP grade. The specific surface area was calculated from the adsorption isotherms by using the BET method.

2.2.2. UV–vis absorption spectra

The UV–vis absorption spectra were obtained with a Varian Cary III UV–vis spectrophotometer coupled with an integration sphere for diffuse reflectance studies. A sample of MgO with a 100% reflectance was used as a reference.

2.2.3. Raman spectroscopy

The Near-infrared Fourier-transform Raman spectroscopic measurements were performed in a Thermo Nicolet ALMEGA dispersive Raman spectrometer equipped with a diode-pumped Nd:YAG laser with an emission wavelength of 1064 nm. The beam was doubly focused on a sample mounted in a capillary tube. The light scattered at 90° over the sample was focused on the entrance slit of a double monochromator; and detected by a Peltier-cooled photomultiplier attached to a phonon counter.

2.2.4. X-ray diffraction and Rietveld refinement

The X-ray diffraction data were obtained at room temperature in a Bruker Advance D-8 diffractometer with a Cu Kα radiation and a graphite secondary beam monochromator. The intensities were obtained in the 2θ ranges between 20 and 110° with a step of 0.05°; and a measuring time of 0.5 s per point. The crystalline structures were refined by using the Rietica (DBW3.2) software from the X-ray and neutron powder diffraction patterns [26]. The tetragonal structure was refined with a tetragonal unit cell with the symmetry described by the $I4_1/amd$ group.

2.2.5. Catalytic activity

The photodegradation experiments were carried out at room temperature. Two hundred and fifty milligrams of catalyst were added to a flask containing an aqueous solution (250 mL) containing 30 ppm of 2,4-dichlorophenoxyacetic acid. The solution was maintained under stirring for 15 min in the dark until the adsorption–desorption equilibrium was reached; then it was irradiated in a closed box with a UV Pen-Ray (UVP) lamp, which emits a λ radiation equal to 254 nm with an emission of 2000 $\mu W/cm^2$. The reaction rate was followed by sampling every 15 min; and then analyzed in a Varian UV–vis spectrophotometer, model Cary-III. The concentration of the 2,4-diclorophenoxyacetic acid was calculated from the adsorption band at 229 nm by applying the Lambert–Beer equation.

3. Results and discussion

3.1. Specific surface area

The specific surface areas of the samples annealed at 673 K are reported in Table 1. It can be seen that the addition of cerium nitrate to the titania gel increases notably the BET specific surface area, from 73 m^2/g, for the bare TiO_2 sample, to 136–174 m^2/g, for the TiO_2–CeO_2 catalysts (Table 1). These results suggested that the hydrolysis-condensation gelling reactions of the titanium alkoxide were perturbed by the presence of cerium, forming, as a consequence, large specific surface areas. One of the advantages of the preparation of doped-titania by the sol–gel method is that the specific surface areas can be increased depending on the nature of the doping agent [21–24]. The mechanism by which the BET specific surface area increases is not well established; however, we can expect the substitution of some Ti^{4+} by Ce^{4+} cations which form (Ti–O–Ce bonds which affect the (Ti–OH polymerization–condensation reactions. According to the aforementioned, remarkable modifications in the textural properties, as it has been recently reported on cerium-doped titania, are obtained [27].

3.2. UV–vis spectroscopy

The band gap energy (E_g) of the samples were estimated from the UV absorption spectra (Fig. 1) taking into account that $\alpha(E) \propto (E-E_g)^{m/2}$, where $\alpha(E)$ is the absorption coefficient for a photon of energy E, and $m = 1$ for an indirect transition between bands [28]. The band gap energies calculated by a linear fit of the slope to the abscissa are reported in Table 1; and they diminish from 3.14 eV, for the bare TiO_2, to 2.47 eV, for the TiO_2–CeO_2-

Table 1
Specific surface area and band gap energy for the TiO_2–CeO_2 (673 K) samples

Substrate	Surface area ($m^2\ g^{-1}$)	λ (nm)	E_g (eV)
TiO_2	73	388	3.14
TiO_2–CeO_2-2.5%	167	403	3.00
TiO_2–CeO_2-5.0%	136	491	2.52
TiO_2–CeO_2-7.5%	137	497	2.49
TiO_2–CeO_2-10.0%	174	502	2.47

E_g: band gap energy.

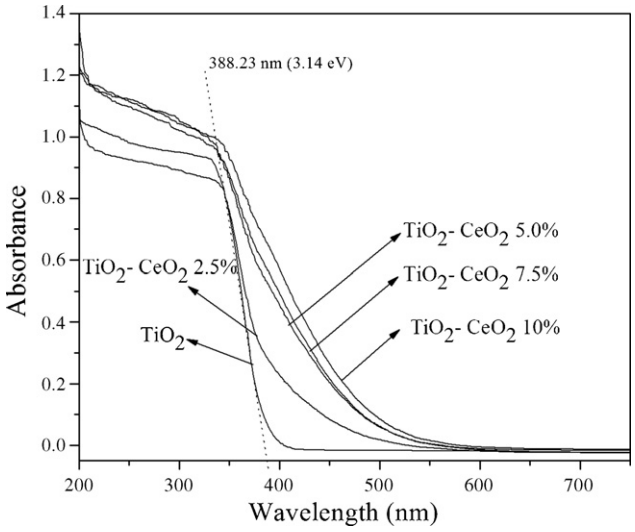

Fig. 1. UV–vis spectra for the TiO_2–CeO_2 samples as a function of the cerium oxide content.

10% sample. It is evident that cerium oxide modifies the bulk semiconductor properties of the TiO_2. The shift of the E_g band gap to a lower energy can be attributed to the incorporation of Ce^{4+} cations, which substitute some Ti^{4+} cations.

3.3. Raman spectroscopy

The Raman spectra for the TiO_2, TiO_2–CeO_2 and cerium oxide (commercial reference) samples in the 300–750 cm^{-1} region are presented in Fig. 2. The Raman spectra for the TiO_2 and TiO_2–CeO_2 catalysts show the peaks assigned to the anatase phase [29]. A 4-cm^{-1} shift to higher energy peaks, 392 and 511 cm^{-1}, respectively, can be seen in the titania–cerium oxide semiconductor. The (Ti–O–Ti) energy bonds of the anatase phase are perturbed by the presence of cerium oxide, which suggests some substitutions of the Ti^{4+} by Ce^{4+} forming (Ti–O–Ce) bonds in the titania structure; as it has been suggested by theoretical computations elsewhere [27].

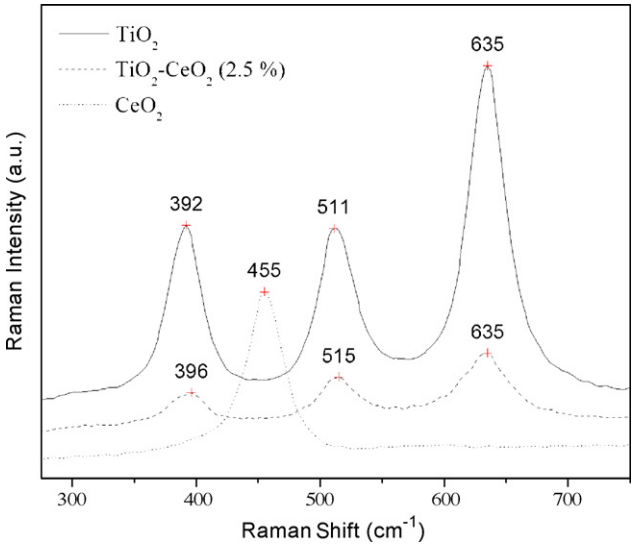

Fig. 2. Raman spectra for the TiO_2, TiO_2–CeO_2 and CeO_2 samples in the 300–750 cm^{-1} region.

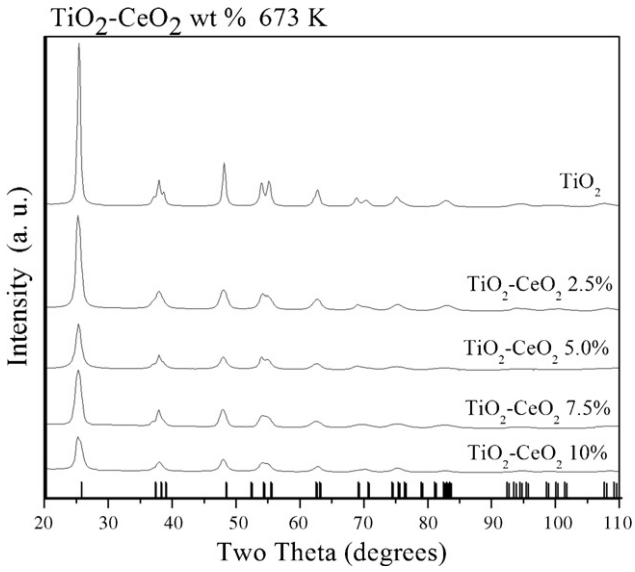

Fig. 3. XRD spectra Rietveld refinements for the TiO_2–CeO_2 samples as a function of the cerium oxide content. Tick marks correspond to anatase.

3.4. X-ray diffraction patterns

The XRD spectra for the TiO_2–CeO_2 mixed oxide semiconductors showed anatase as the crystalline phase. The presence of cerium oxide stabilizes the anatase phase. Peaks identifying the rutile phase as well as cerium oxide are not observed (Fig. 3). The samples contain up to 10 wt.% of cerium oxide; and at such contents, the rare earth oxide should be detected. The absence of cerium oxide in the XRD peaks suggests that it could be in the mixed oxide as a kind of nanostructured conglomerates deposited on the titania surface. The size of such conglomerates was too small; and hence they cannot be detected due to the low resolution of the XRD spectroscopy for the supported nanocrystalline structures. On the other hand, as it has been supported by the modification of the E_g band gap in the TiO_2–CeO_2 mixed oxides, the insertion of some Ce^{+4} in the titania framework cannot be discarded. The spectra in Fig. 3 show that the intensity of the peak at $2\theta = 25.2$, assigned to the anatase (1 0 1) plane diminishes as the cerium oxide content increases. The values of the crystalline size calculated from the Rietveld refinement are reported in Table 2; and they correspond to nanocrystalline structures. The smallest crystallite size was

Table 2
Rietveld refinement data for TiO_2–CeO_2 samples

Substrate	Anatase (wt.%)	Crystallite size (nm)	C_{dTi} (%)	RWP
TiO_2	100	33.0 (19.4)	1.6	6.02
TiO_2–CeO_2-2.5%	100	21.4 (5.4)	45.6	10.89
TiO_2–CeO_2-5.0%	100	8.4 (4.1)	3.6	17.13
TiO_2–CeO_2-7.5%	100	11.4 (4.0)	4.0	13.47
TiO_2–CeO_2-10%	100	21.0 (10.7)	14.5	16.73

The numbers in parentheses correspond to the standard deviation. C_{dTi}: titanium deficiency per unit cell (%), RWP: weight powder porfile R-factor.

obtained in the TiO_2–CeO_2-5% and TiO_2–CeO_2-7.5% catalysts with 8.4 and 11.4 nm, respectively. However, at a higher or lower cerium content the crystallite size increases; and the TiO_2–CeO_2 catalysts at 2.5 and 10 wt.% CeO_2 shows the largest crystallite size of the semiconductors (21.4–21.0 nm). These results showed that by doping TiO_2 with cerium, a minimum in the crystallite size at cerium contents of 5.0 wt.% was obtained.

The Rietica (DBW3.2) software used for the Rietveld refinements enabled us to calculate the number of $[V^{+}_{Ti^{4+}}]$ deficiencies in the titania–ceria samples. In Table 2, it can be seen that the $[V^{+}_{Ti^{4+}}]$ deficiencies reported as % per unit cell, showed a minimum for the catalysts with 5.0 and 7.5 wt.% CeO_2 (3.6 and 4.00% $[V^{+}_{Ti^{4+}}]$); meanwhile, for the semiconductors with 10 wt.% CeO_2; and for the bare TiO_2, the number of titanium defects is of 14.5 and 1.6% $[V^{+}_{Ti^{4+}}]$, respectively.

3.5. Catalytic activity

The activities of the catalysts were evaluated in the photodegradation of the 2,4-dichlorophenoxyacetic acid at room temperature. The photodegradation of the substrate was followed by the UV absorption band at 229 nm. The evolution of the 2,4-dichlorophenoxyacetic acid as a function of time is represent in Fig. 4. From the data of these curves, the apparent rate constant, K, was calculated by the Integral Method for a irreversible monomolecular first order reaction [30]:

$$-r_A = -\frac{dC_A}{dt} = KC_A$$

If the batch reactor works at constant density, then

$$\ln\left[\frac{C_A}{C_{Ao}}\right] = -kt$$

where C_A is the concentration at time t and C_{Ao} is the initial concentration.

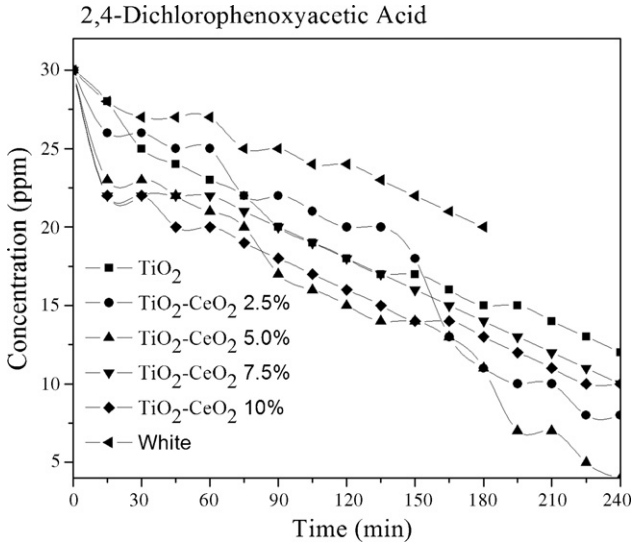

Fig. 4. Photodecomposition of the 2,4-dichlorophenoxyacetic acid as a function of time for the various TiO_2–CeO_2 photocatalysts.

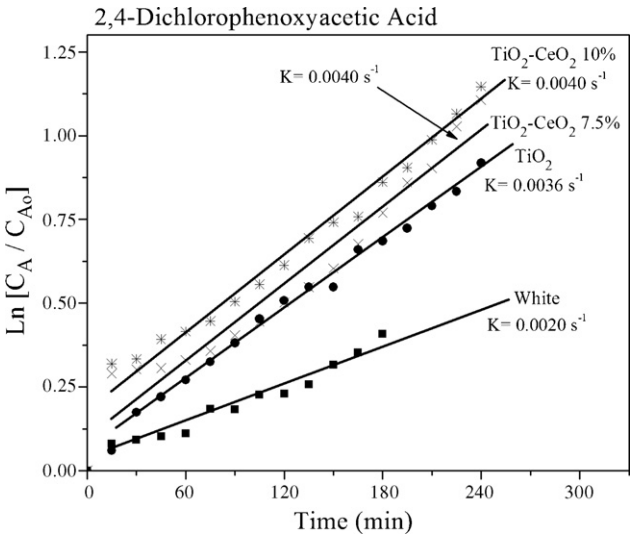

Fig. 5. Kinetic constant for the 2,4-dichlorophenoxyacetic acid decomposition.

An acceptable linearity was obtained by applying the first order kinetic equation (Fig. 5). The values calculated from the selected slopes are reported in Table 3. A maximum in the constant rate was obtained for the sample with 5.0 wt.% CeO_2 ($k = 0.0044\ s^{-1}$).

4. Discussion

One of the most important results related to the modifications of the physicochemical properties of the titania in the TiO_2–CeO_2 mixed oxides is shown in Fig. 6. The graphics of the variation of the E_g band gap as a function of the cerium content showed that the lowest band gap energy (E_g) of the semiconductors corresponds to that in the solids with the highest cerium content. The E_g energy band diminishes in the catalysts with 5 wt.% CeO_2 (2.52 eV); and it is maintained around this value for the 7 and 10 wt.% CeO_2 catalysts. At such concentrations, the maximum substitution of Ti^{4+} by Ce^{4+} cations could be reached; and hence the E_g band gap remains practically constant. These results do not imply that all the cerium added to the titania substituted the Ti^{4+} cations in the titania framework. It illustrates that the maximum substitution, probably just a few titanium cations, is reached with such cerium contents. In fact, we cannot expect a high substitution of Ti^{4+} by Ce^{4+} cations, since the cationic ratio of Ti^{4+} is lower (61 pm) than that of Ce^{4+} (80 pm) [31].

Table 3
Photoactivity for the 2,4-dichlorophenoxyacetic acid decomposition on the TiO_2–CeO_2 mixed oxides

Substrate	K (s^{-1})	Conversion after 4 h (%)
White	0.0020	34 (3 h)
TiO_2	0.0036	60
TiO_2–CeO_2-2.5%	0.0030	74
TiO_2–CeO_2-5.0%	0.0044	87
TiO_2–CeO_2-7.5%	0.0040	67
TiO_2–CeO_2-10.0%	0.0040	68

K: kinetic constant.

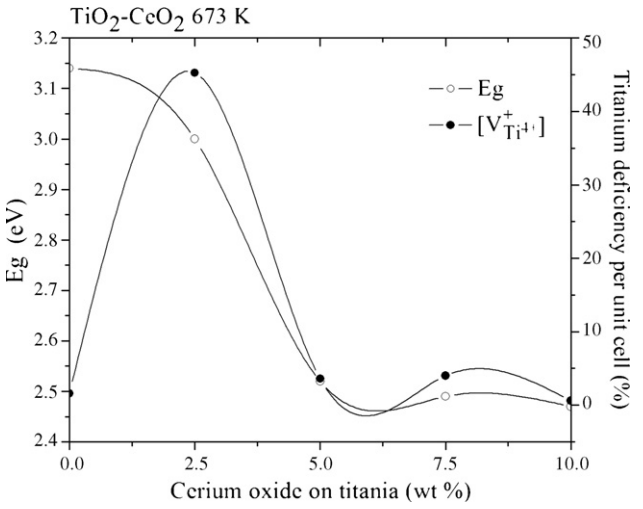

Fig. 6. Band gap energy and titanium deficiency as a function of the cerium oxide content in the TiO_2–CeO_2 samples.

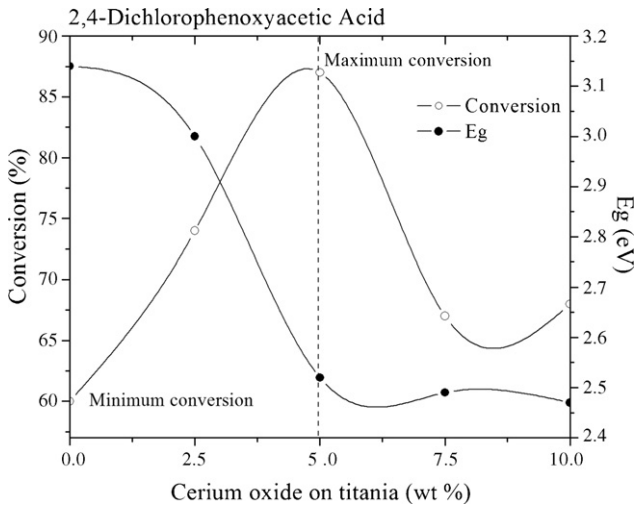

Fig. 7. Conversion and band gap energy as a function of the cerium oxide content in the TiO_2–CeO_2 samples.

However, some evidence of the incorporation of Ce^{4+} is given by the Raman spectrum for the TiO_2–CeO_2-2.5% sample where the shift of the bands at 392 and 511 cm^{-1} denotes the perturbation of the anatase structure by the presence of dopants; in this case Ce^{4+} (Fig. 2).

As it was mentioned above, the number of $[V^{+}_{Ti^{4+}}]$ deficiencies in the titania–ceria oxides can be calculated from the Rietveld refinement data. In Fig. 6 it is plotted the number of $[V^{+}_{Ti^{4+}}]$ deficiencies in the semiconductors as a function of the cerium oxide content. It is remarkable the superimposition of the band gap energy (E_g) values with the number of $[V^{+}_{Ti^{4+}}]$ deficiencies. The Ce^{4+} cations, before being transformed into cerium oxide, act as a doping impurity in the titania framework lowering the E_g band gap. On the other hand, it has been reported that when titania is synthesized by the sol–gel method, a large number of $[V^{+}_{Ti^{4+}}]$ deficiencies are generated, i.e. the Ti^{+4} occupancy concentration (%) was strongly altered by the stoichiometric composition. These Ti^{+4} deficiencies are attributed to the large amounts of OH^{-} trapped in the titania framework [32,33]. The diminution in the generated $[V^{+}_{Ti^{4+}}]$ deficiencies as the cerium oxide content increases, can be due to an important diminution of the hydroxylation of the titania gel. The hydrolysis-condensation reactions of titanium are strongly affected by the presence of cerium nitrate in the TiO_2 gelling medium. In fact, two different phenomena are the responsible for the band gap energy (E_g) diminution (doping); and for the diminution of the Ti^{4+} occupancy. However, they are parallel effects (Fig. 6); and the occurrence between the E_g band gap and the $[V^{+}_{Ti^{4+}}]$ occupancy cannot be discarded.

The correlation among the photocatalytic activity, the E_g band gap and the Ti^{+4} occupancy (%) are shown in Figs. 7 and 8. The catalyst showing the maximum activity was the one with the lowest E_g band gap (TiO_2–CeO_2-5.0%); as well as with the lowest $[V^{+}_{Ti^{4+}}]$ occupancy.

The anatase crystallite size calculated from the Rietveld refinement data (Table 2) was plotted as a function of the cerium content and compared with the photocatalytic activity. In Fig. 9,

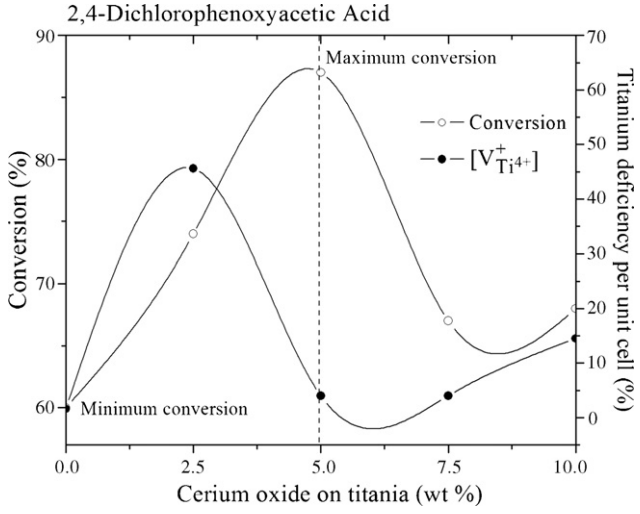

Fig. 8. Conversion and titanium deficiency as a function of the cerium oxide content in the TiO_2–CeO_2 samples.

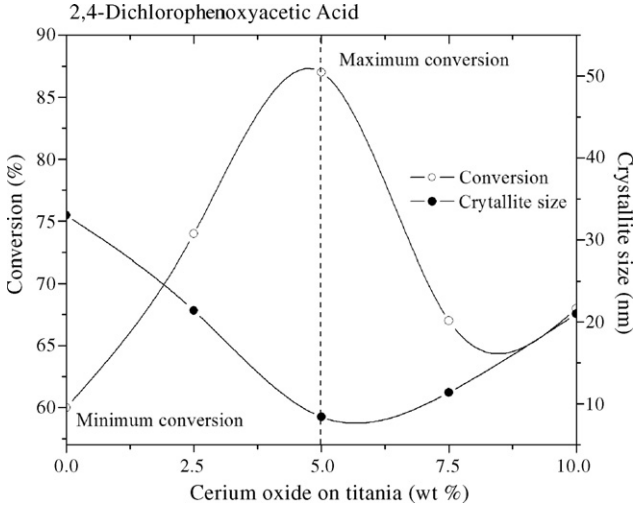

Fig. 9. Conversion and average crystallite size as a function of the cerium oxide content in the TiO_2–CeO_2 samples.

it can be seen that the maximum activity corresponds to the catalyst with the smallest crystallite size (TiO_2–CeO_2-5.0%). A good correlation between the titania crystallite size and the photoactivity was observed. These satisfactory results enabled us to propose that, for the TiO_2–CeO_2 mixed oxides prepared by the sol–gel method, the nanostructure of the mixed oxides is the main factor affecting the catalytic activity. It should be noted that the catalyst with the highest activity not only showed the lowest E_g band gap but also the lowest $[V^+_{Ti^{4+}}]$ deficiency. Then, if a correlation among these three physical properties (E_g band gap, $[V^+_{Ti^{4+}}]$ deficiency and photocatalytic activity) cannot be clearly seen, the possible correlation among them cannot be discarded at all. In this paper we present an important correlation between the photoactivity of doped-titania and the physical and photophysical properties of the mixed semiconductor.

We mentioned that only some of the Ce^{4+} cations can be incorporated into the titania host semiconductor; and to this incorporation was attributed the modifications in the physical and photophysical properties of the TiO_2–CeO_2 semiconductors. The XRD data do not show any characteristic peaks assigned to the formation of CeO_2. It was then assumed that cerium oxides should be found as highly dispersed CeO_2 particles in TiO_2. In such a case, the well established $Ce^{4+}/Ce3^+$ redox pair can play an additional role in the photocatalytic properties. The role of the redox process in the photodegradation of dyes has been recently reported by Xie and Yuan [19]. The Ce^{4+} species acts as an electron scavenger to trap the excited electrons of the organic molecule. The electrons trapped by the Ce^{4+} cations are then transferred to the surrounding O_2 by means of the redox reaction $Ce^{4+} + e \rightarrow Ce^{3+}$; and $Ce^{3+} + O_2 \rightarrow Ce^{4+} + O_2^{\bullet}$, where the $O_2^{\bullet}$ species plays an important role in the overall process of the organic molecule oxidation. The contribution of this redox process in the degradation of the 2,4-dichlorophenoxyacetic acid could not be evaluated in our catalytic system. However, if it contributes to the overall reaction, it could be related to the physical and photophysical properties of the mixed oxide semiconductors of the present work. The quantitative evaluation of the $Ce^{4+}/Ce3^+$ pair and their effects on the E_g band gap, crystallite size and/or $[V^+_{Ti^{4+}}]$ deficiency for the TiO_2–CeO_2 semiconductors, are underway; and it will be the matter of a subsequent contribution.

5. Conclusions

This study shows the modifications in the physical and photocatalytic properties of doped-titania prepared by co-gelling titanium alkoxide and cerium nitrate. The presence of cerium oxide in the titania gelling medium increases the specific surface area. By means of the UV–vis and XRD spectroscopies, it is shown that the band gap energy (E_g) as well as the number of the $[V^+_{Ti^{4+}}]$ deficiencies in the solids diminishes as the cerium oxide content increases. The nanostructured materials which showed titania crystallite sizes between 21.4 and 8.4 nm were obtained by this preparation method. The results in the photocatalytic activity for the 2,4-dichlorophenoxyacetic acid degradation, showed that in the TiO_2–CeO_2 mixed oxide, the highest activity is obtained in the catalyst showing the lowest band gap energy (E_g) and the lowest number of $[V^+_{Ti^{4+}}]$ deficiencies. A strong dependence between the photoactivity and the crystallite size was exposed: the smaller the crystallite size the higher the photocatalytic activity. The contribution of the Ce^{4+}/Ce^{3+} redox pair in the herbicide degradation was also taken into account; and its importance in the overall reaction is considered as a result of the physical and photophysical properties of the TiO_2–CeO_2 mixed oxides.

Acknowledgements

We thank the support given by the SEP-FIES programs. F. Galindo thanks CONACYT for the grants awarded.

References

[1] M. Anpo, Pure Appl. Chem. 72 (2000) 1265.
[2] J.E. Herrmann, Catal. Today 112 (2006) 73.
[3] M.I. Litter, Appl. Catal. B: Environ. 23 (1999) 89.
[4] J.M. Herrmannn, Topics Catal. 34 (2005) 49.
[5] K. Rajeshwar, C.R. Chenthamaraskshan, S. Goering, M. Djukic, Pure Appl. Chem. 73 (2001) 1849.
[6] Y. Cao, X. Zhang, W. Yang, H. Du, Y. Bai, T. Li, J. Yao, Chem. Mater. 12 (2000) 3445.
[7] K. Vinodgopal, P.V. Kamat, Environ. Sci. Technol. 29 (1995) 841.
[8] S.P. Fen, G.W. Meng, L.D. Zhang, Chin. Sci. Bull. 43 (1998) 1613.
[9] X. Fu, L.A. Clark, Q. Yang, M.A. Anderson, Environ. Sci. Technol. 30 (1996) 647.
[10] J. Araña, O. González Díaz, M. Miranda Saracho, J.M. Doña Rodríguez, J.A. Herrera Melián, J. Pérez Peña, Appl. Catal. B: Environ. 36 (2002) 113.
[11] J.A. Navío, G. Colon, M. Macias, C. Real, M.I. Litter, Appl. Catal. A: General 177 (1999) 11.
[12] J.A. Navio, J.J. Testa, P. Djedjeian, J.R. Padron, D. Rodriguez, M.I. Litter, Appl. Catal A: General 178 (1999) 191.
[13] C. Anderson, A.J. Bard, J. Phys. Chem. B 101 (1997) 2611.
[14] S.K. Poznyak, D.V. Talapin, A.I. Kulak, J. Phys. Chem. B 105 (2001) 4616.
[15] D. Shchukin, S. Poznyak, A. Kulak, P. Pichat, J. Photochem. Photobiol. A: Chem. 162 (2004) 423.
[16] J. Aguado, R. van Grieken, M.J. Lopez-Muñoz, J. Marugan, Appl. Catal. A: General 312 (2006) 202.
[17] B. Malinowska, J. Walendziewski, D. Robert, J.W. Weber, M. stolarski, Appl. Catal. B: Environ. 46 (2003) 441.
[18] K. Jung, S.B. Park, Mater. Lett. 58 (2004) 2897.
[19] Y. Xie, C. Yuan, Appl. Catal. B: Environ. 46 (2003) 251.
[20] T. Lopez, R. Gomez, E. Sanchez, F. Tzompantzi, L. Vera, J. Sol–Gel Sci. Technol. 22 (2001) 99.
[21] T. Lopez, J. Hernandez-Ventura, R. Gomez, E. Sanchez, X. Bokhimi, A. Garcia, J. Mol. Catal. A: Chem. 167 (2001) 101.
[22] J.A. Wang, R. Lima-Bellesteros, T. Lopez, A. Moreno, R. Gomez, O. Novaro, X. Bokhimi, J. Phys. Chem. B 105 (2001) 9692.
[23] R. Gomez, T. Lopez, E. Ortiz-Islas, J. Navrrete, E. Sanchez, F. Tzompantzi, X. Bokhimi, J. Mol. Catal. A: Chem. 193 (2003) 217.
[24] V. Rodríguez-González, A. Moreno-Rodríguez, F. Tzompantzi, R. Gómez, J. Photochem. Photobiol. A: Chem. 193 (2008) 266.
[25] A. Trovarelli (Ed.), Catalysis by Ceria and Related Materials, vol. 2, Imperial College Press, London, 2005, Catalytic Science Series.
[26] http://www.ccp14.ac.uk.
[27] T. Lopez, F. Rojas, R. Alexander-Katz, F. Galindo, A. Balankin, A. Buljan, J. Solid State Chem. 177 (2004) 1873.
[28] N. Serpone, E. Pelizzetti, Photocatalysis: Fundamentals and Applications, John Wiley, New York, 1989, pp. 60–61.

[29] Mineral Raman DataBase, Laboratory of Photoinduced Effects, Vibrational and X Spectroscopies-PHEVIX, Dipartimento di Fisica, Università degli Studi di Parma, Italy, http://www.fis.unipr.it/phevix/ramandb.html.
[30] O. Levenspiel, Chemical Reaction Engineering, John Wiley & Sons, Inc., New York, 1990, p. 50.
[31] (a) J.E. Huheey, Inorganic Chemistry, Harper & Row Pub. Inc., New York, 1978, p. 74;
(b) J.E. Huheey, Inorganic Chemistry, Harper & Row Pub. Inc., New York, 1978, pp. 115–117.
[32] X. Bokhimi, A. Morales, O. Novaro, T. López, E. Sanchez, R. Gomez, J. Mater. Sci. Res. 10 (1995) 2788.
[33] E. Sanchez, T. Lopez, R. Gomez, X. Bokhimi, A. Morales, O. Novaro, J. Solid State Chem. 122 (1996) 309.